AD-A097 772 NAVAL RESEARCH LAB WASHINGTON DC F/G 20/8
FAST ION STOPPING POWER IN DENSE, IONIZED PLASMAS.(U)
APR 81 J E ROGERSON
UNCLASSIFIED NRL-MR-4485 NL

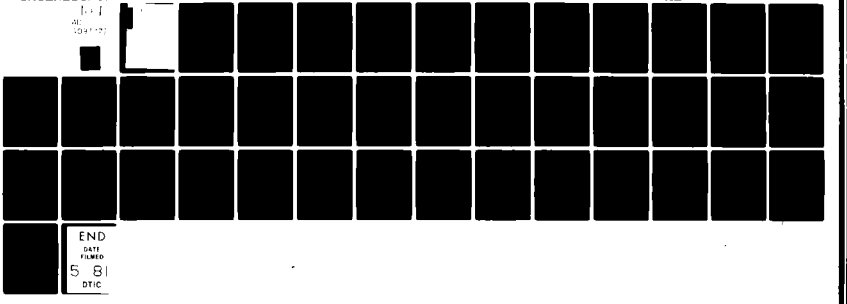

END
DATE FILMED
5 81
DTIC

SECURITY CLASSIFICATION OF THIS PAGE (When Data Entered)

REPORT DOCUMENTATION PAGE	READ INSTRUCTIONS BEFORE COMPLETING FORM
1. REPORT NUMBER: NRL Memorandum Report 4485 AD-A097732	2. GOVT ACCESSION NO. / 3. RECIPIENT'S CATALOG NUMBER
4. TITLE (and Subtitle): FAST ION STOPPING POWER IN DENSE, IONIZED PLASMAS	5. TYPE OF REPORT & PERIOD COVERED: Interim report on a continuing NRL problem.
	6. PERFORMING ORG. REPORT NUMBER
7. AUTHOR(s): J. E. Rogerson	8. CONTRACT OR GRANT NUMBER(s)
9. PERFORMING ORGANIZATION NAME AND ADDRESS: Naval Research Laboratory, Washington, DC 20375	10. PROGRAM ELEMENT, PROJECT, TASK AREA & WORK UNIT NUMBERS: 62704H; 47-0857-0-1
11. CONTROLLING OFFICE NAME AND ADDRESS: Defense Nuclear Agency, Washington, DC 20305	12. REPORT DATE: April 17, 1981
	13. NUMBER OF PAGES: 40
14. MONITORING AGENCY NAME & ADDRESS(if different from Controlling Office)	15. SECURITY CLASS. (of this report): UNCLASSIFIED
	15a. DECLASSIFICATION/DOWNGRADING SCHEDULE

16. DISTRIBUTION STATEMENT (of this Report)

Approved for public release; distribution unlimited.

17. DISTRIBUTION STATEMENT (of the abstract entered in Block 20, if different from Report)

18. SUPPLEMENTARY NOTES

19. KEY WORDS (Continue on reverse side if necessary and identify by block number)

Dense plasmas
Ionized plasmas
Stopping power

20. ABSTRACT (Continue on reverse side if necessary and identify by block number)

A model is presented for calculating stopping cross sections for ions in ionized plasma targets. This approach utilizes a local oscillator model to calculate stopping power by bound electrons. Results obtained from this formulation are presented and compared with other calculations.

DD FORM 1 JAN 73 1473 EDITION OF 1 NOV 65 IS OBSOLETE
S/N 0102-014-6601

SECURITY CLASSIFICATION OF THIS PAGE (When Data Entered)

CONTENTS

FAST ION STOPPING POWER IN DENSE, IONIZED PLASMAS

I. INTRODUCTION

The growing interest in ion beams as drivers in Inertial Confinement Fusion (ICF) has created a need for reliable methods of calculating beam stopping power as a function of the temperature, density, and composition of the target material. Such information is essential for the optimal design of ICF target pellet configurations. Because the slowing down process can generate energetic x-rays, it is also of interest in simulation studies for nuclear weapons effect. It is therefore evident that ion stopping power studies are useful in a number of areas of interest to the scientific and the military communities.

In this report, a "local oscillator" model for bound electron stopping power is described and applied with good success to a number of cold target calculations. This model is then extended to partially ionized atoms and combined with free electron stopping power equations to calculate total electron stopping power results for target plasmas of given density, temperature, and degree of ionization. Results are compared with other calculations.

II. BOUND ELECTRON STOPPING POWER

Two widely used models in the calculation of the stopping power of bound atomic electrons are the LSS model[1], which is valid at low velocities, and the Bethe theory, which applies to high velocity projectiles. These are complementary models and can be used to span the entire velocity range; for example, Mehlhorn[2] computes results for both models at a given velocity and takes the lower of the two values as the stopping cross section.

Manuscript submitted January 28, 1981.

The chief difficulty in applying the Bethe theory is obtaining the average ionization potential $\bar{I}$. A calculation of this quantity is a tedious exercise; hence, various scaling mechanisms have been proposed to estimate $\bar{I}$ [e.g., Mosher[3], Mehlhorn[2]]; to circumvent this difficulty, the "local oscillator model" (LOM) [Nesbet and Ziegler[4]] was chosen to represent stopping by bound electrons. In the LOM, the bound electron stopping cross section is given by

$$S_b(v) = \frac{4\pi Z_1^2 e^4}{mV^2} \int 4\pi r^2 \rho(r) K_o(\tau)\, dr. \tag{1}$$

where Z_1 is the effective charge of the projectile ion, e and m are the electron charge and mass, V is the projectile velocity, $\rho(r)$ is the local bound electron density in the target atom, and $K_o(\tau)$ is a modified zero order Bessel function.

$$\tau = \hbar\, \omega_o\, (r)/mV^2. \tag{2}$$

where $\hbar$ is Planck's constant divided by 2π, and $\omega_o(r)$ is the local plasma frequency at radius r within the atom.

There are three assumptions underlying the LOM[4]. The first is that a loss function can be defined dependent only on the local electron density in the target atom. The second is that the longitudinal dielectric response can be represented by $\varepsilon(\omega)$ with a single zero at $\omega \sim \omega_o$, subject to the high frequency condition

$$\varepsilon(\omega) \sim 1 - \omega_o^2/\omega^2 \tag{3}$$

appropriate to free electrons. The third assumption is that the induced polarization charge is spread out from the ion trajectory to some finite radius of the order of the de Broglie wavelength $\hbar/mV$. This last assumption is

justified by the adiabatic argument that energy will be transferred only to electrons with velocity less than V. A wave packet with momentum of order mV would have a spatial spread of order $\hbar/mV$.

The electron density $\rho(r)$ is taken from the Thomas-Fermi (TF) model proposed by Zink[5]. For an isolated, zero-temperature atom, the TF potential is assumed to have the form

$$V_i = Ze/r(1 + Ar)^2, \tag{4}$$

where the parameter A is determined by the condition

$$\int_0^\infty \rho_i(r)\, 4\pi r^2\, dr = Z, \tag{5}$$

$\rho_i(r)$ is given by the TF equation

$$\rho_i(r) = \left(\frac{8\pi}{3h^3}\right) \left(2\, meV_i\right)^{3/2}, \tag{6}$$

and Z is the number of electrons bound to the nucleus. The solution is

$$A = 1.14 \times 10^8\ Z^{1/3}\ cm^{-1}. \tag{7}$$

This leads to the following expression for the TF electron density of an isolated atom at zero temperature;

$$\rho(r) = 3ZA^2/2\pi r\ (1 + Ar)^4. \tag{8}$$

As shown by Zink[5], this procedure can be applied to a partially ionized atom. The atomic volume is divided into two regions. The inner region around the nucleus, bounded by r_1, contains the bound electrons and has a high electron density; the outer region contains free electrons and has a low density. The outer region is defined by the interval $r_1 \leq r \leq R$, where R is the radius of an unionized atom at the given density of the material. The electron density is given by

$$\rho(r) = \frac{Z^*}{\frac{4}{3}\pi R^3} + \frac{3Z A^2}{2\pi r(1+AR)^4} ; \quad 0 \le r \le r_1$$

$$\rho(r) = \frac{Z^*}{\frac{4}{3}\pi R^3} ; \quad r_1 \le r \le R \tag{9}$$

where Z^* is the number of free electrons.

Zink[5] establishes the following relationship between Z* and r_1:

$$Z^* = \frac{2 Z A r_1}{(1+Ar_1)^3} + \frac{Z}{(1+Ar_1)^2} . \tag{10}$$

Thus, if either Z* or r_1 is known, the TF electron density can be written for the ionized atom.

The approach taken in this calculation is to solve an LTE Saha model for the average charge $\bar{Z}$ of the atoms as a function of density and electron temperature. Then Z* is set equal to $\bar{Z}$, and a TF electron density can be written for an "average atom" in the plasma. In this way, the bound electron stopping power in a partially ionized plasma can be computed.

The relation given by Brown and Moak[6] is used to define the effective charge Z_1 of the projectile atom with nuclear charge Zp;

$$Z_1/Zp = 1.0 - 1.034 \exp(-V/V_\ell), \tag{11}$$

where

$$V_\ell = Z_p^{0.69} (e^2/\hbar). \tag{12}$$

This relation was obtained by plotting several hundred data points for effective charge and performing a least-squares fit to the results. It was found empirically in applying the LOM model to cold targets that good agreement with standard results[7,8] was obtained with Z_1 replaced by Z_p, the projectile atomic number in Eq. (1), and the result scaled by[9]

$$f = (\gamma/\gamma_p)^2 , \tag{13}$$

where γ is the result of applying Eq. (11) to the incident ion, and γ_p is the result of Eq. (11) for a proton at the same velocity (with $V_\ell = e^2/\hbar$). For incident protons, Zeff/Z = 1.0 gave good results for the energies considered.

The integral in Eq. (1) is taken over the radius of the atom (R for neutral atoms and r_1 for ionized atoms). Low energy projectiles do not penetrate the atomic electron cloud very deeply; hence, only a few points near the outer edge of the radial grid contribute significantly to the integral. Also, in reality, the radius, or boundary, of the atom is not sharply defined. At low velocity, from Eq. (11), the projectile atom has a small effective charge; it retains most of its own electron charge cloud which increases the size of the interaction region with the target atom. It is therefore possible to omit significant contributions to the stopping cross section at low velocities by using Eq. (1). Indeed, it sometimes occurs that, at low energy, the results given by Eq. (1) are too low as compared with accepted values for stopping cross sections e.g., Andersen and Ziegler[7] . Thus, there may be a physical and numerical difficulty with Eq. (1).

According to Land and Brennan[9], for velocities below V_ℓ the stopping cross section can be taken to be linear in velocity. Therefore, in this regime, a scaled cross section is calculated from

$$S_b(V) = S_b(V_\ell) * (V/V_\ell), \quad V < V_\ell, \tag{14}$$

where $S_b(V_\ell)$ is calculated from Eq. (1). The stopping cross section is then taken to be the larger of the results of Eq. (1) or Eq. (14).

For velocities larger than V_ℓ, the projectile has a higher effective charge and penetrates more deeply into the target atomic electron cloud, and the smeared out boundary problem does not arise.

Some results from this model for stopping cross sections for hydrogen atoms in cold, solid density targets are shown in Figure 1 and compared with the results of Andersen and Ziegler[7]. In Figure 1a, the agreement is very good over the entire energy range for an Aℓ target. In Figure 1b, for an Fe target, the agreement is good, except in the 100-200 keV range, where the LOM result is about 20 percent low. For the Au target in Figure 1c the errors are about 14 percent or less. The LOM peaks appear to be shifted to lower energy by about 20 keV to 50 keV relative to the reference curves. In the high energy, or Bethe theory, regime, the agreement is very good. As noted earlier, in the LOM model, a calculation of mean ionization potential is not necessary.

In Figures 1d to 1f are shown comparisons of range calculations vs. energy from this model with Andersen and Ziegler[7] results. Good agreement is obtained again except at the lowest energies; this results from an omission of energies below 1 keV in these calculations.

Cold target calculations for C atom projectiles are shown in Figure 2. In Figures 2a and 2b, comparisons with the results of Northcliffe and Schilling[8] for Aℓ and Au targets at solid density are given; good agreement is obtained. Not shown are the range calculations for these situations; they also agree well with Northcliffe and Schilling[8]. Coincidences of the peaks may be noted in Figure 2.

The previous cases dealt with light ion projectiles on heavier atom targets. The situation treated in Figures 3a and 3b is the reverse; here cold target calculations at solid density are presented for U atoms impinging on Aℓ and Au atoms. For comparison, the results of Northcliffe and Schilling[8] and Brueckner and Metzler[10] are also given. In Figure 3a, at low energy, the LOM results agree very well with Northcliffe and Schilling[8] but are much lower than Brueckner and Metzler[10]. As energy increases, however,

the Northcliffe and Schilling[8] results drop much faster than the LOM results, while the Brueckner and Metzler[10] curve approaches the LOM results. In Figure 3b, the Bruckner-Metzler[10] results and the LOM agree very well at all energies, while the Northcliffe and Schilling[8] curve is much lower. As argued by Brueckner and Metzler[10], the Northcliffe-Schilling[8] data for heavy ions at high energy are based on extrapolations from low energy data and are therefore somewhat uncertain. Brueckner and Metzler[10] calculate the bound electron stopping power by using a Thomas Fermi model to evaluate the electronic excitation energies and the Coulomb logarithm term in the stopping power equation; hence, there is some similarity between their model and the LOM. However, they use a different effective charge scaling law which results in a higher effective charge.

III. FREE ELECTRON STOPPING POWER: PLASMA TARGETS

For heated target materials, the atoms become ionized, and stopping due to free electrons must be considered. The free electron stopping cross section is calculated from

$$S_f(V) = \frac{2\pi e^4 Z_1^2 \bar{Z}}{mV^2} F(x) \left\{ \ell n \left(1 + \frac{D^2}{b^2}\right) + \ell n (1 + 4 x^2) \right\} \qquad (15)$$

where $\bar{Z}$ is the average charge of the target ions (currently obtained from a Saha LTE equation-of-state), D is the Debye shielding length, and

$$x = (mV^2/2kT)^{1/2}, \qquad (16)$$

where kT is the electron temperature.

$$F(x) = \mathrm{erf}(x) - 2 x e^{-x^2} / \sqrt{\pi} \qquad (17)$$

The quantity b is the minimum impact parameter for electron-ion scattering and is given by

$$b = \mathrm{MAX}\left\{\frac{Z_1 e^2}{mV^2}, \quad \frac{\hbar}{2mV}\right\}, \tag{18}$$

i.e., the maximum of either the classical or quantum-mechanical impact parameter defined by the uncertainty principle.

The first term in Eq. (15) is the short range ion-electron binary-encounter scattering term and is taken from the work of Campbell[11], who adapted it from Brueckner and Brysk[12]. The second term is the polarization term and is taken from Pines and Bohm[13]. For distances larger than D, the plasma acts as a continuous medium, and distant collisions cause loss of energy by the excitation of plasma oscillations, which appear as an oscillating wake behind the projectile.

As discussed by Mehlhorn[2], the effective charge of the projectile ion will be increased by the plasma free electrons due to increased collisional ionization. A higher relative velocity occurs between ion and plasma than for the cold target. Therefore, in Eqs. (11) and (18), the ion velocity is replaced by the addition of the ion velocity and electron thermal velocity in a random phase manner. The scaling defined by Eq. (13) is also applied to Eq. (15).

In a plasma target, the bound atomic electrons can be screened from the projectile ions by the free electrons. Thus, the LOM must be modified to take this shielding effect into account. For an electron in an isolated atom, the maximum impact parameter is V/ω, where ω is a characteristic frequency of motion[14,15]. Plasma screening limits this parameter to the Debye length D. Eq. (2) can be rewritten

$$\tau = (\hbar/mV) * (\omega_o(r)/V) \ .$$

Whenever $V/\omega_o(r) > D$, τ is taken to be

$$\tau = \hbar/mVD \tag{19}$$

Thus, plasma shielding of the bound electrons is taken into account by limiting the argument of the Bessel function as given by Eq. (19).

For a plasma target at a given temperature and ion density, a Saha LTE model is used to obtain the average ionic charge $\bar{Z}$. Using the LOM as modified for plasma screening in combination with Zink's[5] model for determining Thomas-Fermi electron densities for partially-ionized atoms gives the bound electron stopping cross section. Adding this result to Eq. (15) gives the total electronic stopping cross section.

This formalism has been applied to the stopping power of Au at kT = 200 eV and at 0.01 times solid density ρ_s for carbon ions. The results are shown in Figures 4a and 4b; also given are Mehlhorn's[2] results for comparison. Mehlhorn's $S_b(V)$ results are generally higher, especially at high energy, where the difference is $\sim$ 25 percent. As mentioned earlier, Mehlhorn uses a Bethe model to calculate bound electron stopping at high energy; the differences could be due to different effective $\bar{I}$'s in the two calculations. Also, Mehlhorn ignores plasma shielding effects on the bound electrons, which would lead to smaller values of $S_b(V)$. Figure 4b shows the free electron stopping cross sections; here the agreement is good over the entire energy range. Since free electron stopping clearly dominates the bound electron contribution in this case, the total electronic stopping power is approximately the same for both calculations, especially at the higher energies.

Figure 5 shows a comparison with Brueckner and Metzler[10] for H atoms in an Al target at solid density and at kT = 10 eV and 2 keV. At 2 keV, Al is

completely ionized, and the electronic stopping is totally due to free electrons. The two calculations are in good agreement here. At 10 eV, bound electron stopping cross sections are larger than the free electron cross sections by about 50 percent; hence screening of the bound electrons is important in this case. The Brueckner-Metzler result is about 30 percent lower than the results of this model. As mentioned earlier, they use a different model to calculate bound electron stopping. They take plasma screening into account by using a combination of the Debye length D and the isolated atom maximum impact parameter V/ω.

Figure 6 shows total electronic stopping cross sections for protons on solid density Au at kT = 10 eV and 2 keV; also shown are the Brueckner-Metzler calculations. At 10 eV, stopping by bound electrons dominates the cross sections; the two calculations are in very good agreement. At 2 keV, free electron stopping predominates. The Brueckner-Metzler results are about 20 to 25 percent lower; this is probably due to differences in the models for free electron stopping power.

Figure 7 shows cross section calculations for U ions on a solid density Al target. At kT = 10 eV, there is a wide disparity between these results and the Brueckner-Metzler calculations at low energy; at higher energy, their results are approximately 30 percent lower. At 2 keV, there is a large disagreement in the low energy range, but the results appear to be merging at the high energy end. These differences appear to be explained by the difference in the effective charge scaling laws. According to Brueckner and Metzler, their scaling law can show a ratio $(Z_{eff}/Z)^2$ as large as twice the result of Eq. (11) for energies of few MeV/amu.

Figure 8 shows comparisons with Brueckner and Metzler for U ions at one-tenth solid density Au at kT = 200 eV and 2 keV. The 2 keV results are

similar in appearance to those of Figure 7, and the same statements regarding scaling laws apply. The 200 eV curves are in reasonably good agreement for energies $\geq$ 4 MeV/amu. Free electron stopping dominates by factors of 1.5 to 2 at higher energies.

Nardi, Peleg, and Zinamon[15] (NPZ) have calculated electronic stopping cross sections for protons in Au; comparisons with these results are shown in the next two figures. Figure 9 shows free electron stopping cross sections at solid density and kT = 1 keV. The NPZ results for both collisional and non-collisional plasma dielectric functions are shown; also given are calculations based on Eq. (15) and the Brueckner-Metzler results. The agreement between this model (Eq. (15)) and the NPZ non-collisional results is good over the energy range 1 to 10 MeV. The Brueckner-Metzler curve agrees with the NPZ collisional results at low energy but falls below the other calculations as energy increases; at 10 MeV, the Brueckner-Metzler result is approximately 20 percent lower than the others.

Eq. (15) represents a type of model that NPZ refer to as "binary plus collective", i.e., short range binary collisions plus long range collective effects; at high energies ($\geq$ 4 MeV), they obtained good agreement between this kind of model and their more complex dielectric function models. The results of Eq. (15) as shown in Fig. 9 reinforce their conclusions; in fact, the Eq. (15) results are in excellent agreement with their "binary + Pines-Bohm" result. At low energies, where the projectile velocity is not large compared to the electron thermal velocity, the dielectric function models predict lower cross sections than the binary plus collective models.

Figure 10 shows free electron stopping cross sections for protons in Au at one-hundredth of solid density and kT = 1 keV. The NPZ dielectric function results, calculations based on Eq. (15), and Mehlhorn's[2] dielectric function and binary-plus-collective (i.e., Jackson[14]) results are given. The

dielectric function calculations of NPZ and Mehlhorn agree very well in the 1 to 10 MeV range. Mehlhorn's binary-plus-collective results lie between the dielectric function calculations and the results from Eq. (15). Again there is some disparity at lower energies, but all the curves tend to merge at high energy.

Figure 11 shows free electron stopping cross sections for protons in Au at one-tenth solid density and kT = 50 eV. Results from Eq. (15) are shown along with Mehlhorn's[2] dielectric function calculations and his binary plus-collective calculations. Agreement is good among the three results for energy $\geq$ 3 MeV. This again bears out the conclusion of NPZ and also Mehlhorn that, in this energy range, the binary-plus-collective-oscillations model is in good agreement with more complex dielectric function calculations.

The dependence of this model on electron temperature is displayed in Figures 12 and 13. In both calculations, the cross sections at 10 eV are lower than the cold target cross sections; this is due to shielding of the bound electrons by the free plasma electrons. As the electron temperature rises and the free electron contribution becomes more significant, the cross section rises again so that, at 50 eV, they are larger than the cold target cross sections. At energies above 5 MeV/amu for these calculations; the cross sections continue to rise with increasing kT. At lower energies as kT rises, the cross sections show a decrease. This is due to the function F(x) (defined by Eq. (17)). This function is a measure of the Coulomb interaction between the projectile ion and the plasma electrons and restricts energy losses by the projectile ion only to electrons with velocity lower than the ion velocity. As kT increases, losses by low velocity ions to the plasma decrease.

This initial drop in the stopping power as the temperature rises in the target material is the same trend predicted by Brueckner and Metzler[10];

however, their model predicts a much more severe decrease than this model indicates. This is probably due to differences in the models and in different treatments of the plasma shielding effects.

Calculations with this model which omit this screening effect predict a steady increase of stopping power with electron temperature, as Mehlhorn[2] predicts; there is no initial drop as kT rises above the cold target temperature. Mehlhorn omits this plasma screening effect.

It should be noted that the differences between the cold target and the 1 keV cross sections in Fig. 12 are in good agreement with the results given by NPZ[15] for their cold target and "binary + Pines Bohm".

The effect of density in this model is shown in Fig. 14, where stopping cross sections for U ions in Au and solid density ρ_s and 0.1 ρ_s are given for 10 eV, 100 eV, and 1000 eV. In each case, the lower density target gave higher stopping cross sections. This effect is also predicted by Brueckner and Metzler[10] and Mehlhorn[2].

Mosher[3] has calculated a dimensionless correction term ($\ln \Lambda - \ln \Lambda_s$) which is a measure of the difference between stopping powers for a heated plasma and for a cold, neutral target; he shows the variation of this quantity for targets with Z = 6 and Z = 81 for the range 10 eV $\leq$ kT $\leq$ 1000 eV at several electron densities. In an effort to compare with these results, some of the stopping cross sections calculated here were taken at a given energy, the cold target results at the same energy were subtracted, and the difference divided by the quantity

$$R_N = \frac{4\pi e^4 Z_1^2}{m_e v^2} Z \qquad (20)$$

to obtain a normalized, unitless difference analogous to Mosher's[3].

Results for U projectiles on Au targets at $p = 0.1\ \rho_s$ were chosen for comparison; for this situation, Z = 79, and the product of Z times atomic number density is 4.6×10^{23}; this is reasonably close to his Z = 81, $N = 10^{23}$ case. Calculations were done for energies of 12 MeV/amu and 20 MeV/amu for this model, and similar calculations were done for these energies from the Brueckner-Metzler[10] data. The results are summarized in Table 1.

TABLE 1: U → Au, $p = 0.1\ \rho_s$, $N_e = 10^{23}$

		E = 12 meV/amu		E = 20 MeV/amu	
kT(eV)	Mosher[3]	This model	B-M[10]	This model	B-M[10]
10	∿ 0	- 0.14	- 0.64	- 0.18	- 0.69
100	∿ 0	+ 0.21	- 0.37	+ 0.23	- 0.48
1000	∿ + 4.3	+ 1.68	+ 1.80	+ 1.68	+ 1.75

Mosher's[3] correction term is independent of projectile velocity and depends only on the target plasma. Both the Brueckner-Metzler[10] results and calculations from this model appear to verify this conclusion in this energy range. The model used in this report agrees fairly well with Mosher[3] at 10 eV and at 100 eV and with Brueckner and Metzler at 1000 eV, where Mosher's[3] result is larger by a factor of order 2.5. The Brueckner-Metzler[10] results are much lower than Mosher's[3] at each value of kT.

Mosher[3] also presents results for this correction term for a target Z of 6 and several electron densities. Calculations were done for protons incident on carbon atoms at E = 10 MeV/amu and 20 MeV/amu and at electron densities of 10^{20} and 10^{23}. Comparisons are given in Table 2.

TABLE 2: H → C

	$N_e = 10^{20}$			$N_e = 10^{23}$		
kT (eV)	Mosher[3]	E=10 $\frac{MeV}{amu}$	E=20 $\frac{MeV}{amu}$	Mosher[3]	E=10 $\frac{MeV}{amu}$	E=20 $\frac{MeV}{amu}$
10	∿ 0	+ 3.04	+ 3.08	∿ - 0.5	+ 0.03	+ 0.16
30	∿ + 0.2	+ 3.25	+ 3.25	∿ - 1.0	+ 1.13	+ 1.06
100	∿ + 2.8	+ 5.44	+ 5.50	∿ + 0.4	+ 1.86	+ 1.84
300	∿ + 4.5	+ 5.50	+ 5.50	∿ + 1.7	+ 2.40	+ 2.40
1000	∿ + 6.4	+ 5.34	+ 5.53	∿ + 2.8	+ 2.34	+ 2.44

The results of this model are again approximately independent of velocity in this energy range. Mosher's[3] results for $N_e = 10^{20}$ vary over a much wider range as kT changes; this may be due to a difference of ionization models. The results at $N_e = 10^{23}$ are generally higher than Mosher's[3] except at 1 keV, where they are comparable.

The differences with Mosher's[3] results are probably due to different free electron stopping power models.

IV. CONCLUSIONS

A local oscillator model for bound atomic electron stopping power has been utilized to calculate stopping cross sections for several projectile ions in cold targets; Thomas Fermi electron densities as proposed by Zink[5] were used in the computations. Good agreement with standard results[7,8] were obtained over the entire energy range. Thus the LOM appears to have a solid basis as a model for bound electron stopping power.

Using Zink's[5] formulation, this model was extended to partially ionized atoms and modified to take into account shielding of the bound atomic electrons

by the free plasma electrons. It was then combined with a binary-collisions-plus-collective-oscillations model of free electron stopping power to calculate total electron stopping power in heated plasmas.

In most instances, reasonable agreement with comparison calculations was obtained; hence some confidence in these results are justified.

From an examination of Figures 4 through 11, it is apparent that, in the treatment of free electron stopping power, this model is closer to those of Mehlhorn[2] and NPZ[15] than it is to that of Brueckner and Metzler[10]. Both NPZ and Mehlhorn agree that, in the high energy range, the so-called binary-plus-collective oscillations approach as represented by Eq. (15) yields results in good agreement with more complex dielectric function calculations. There are differences in the treatment of bound electron stopping power: Mehlhorn and NPZ use the Bethe theory, while this report adopts the local oscillator model.

One of the questions still to be settled is the effective charge on the projectile ion. The expression obtained by Brown and Moak[6] was used here, but Brueckner and Metzler[10] adopt an expression that yields a higher effective charge.

Another problem which this model does not address, but which is under study, is the problem of electron degeneracy which arises at densities well above solid densities. Any detailed study of ICF plasmas must include degeneracy effects.

V. ACKNOWLEDGMENTS

The author wishes to thank Dr. V. L. Jacobs and Dr. J. Davis of NRL for valuable discussion. He also wishes to thank Dr. E. Kane of Science Applications, Inc. for valuable discussion of the free electron stopping power problem. He wishes to thank Robert Ernst for assistance in preparing the graphs.

This work was funded by the Defense Nuclear Agency.

REFERENCES

1. J. Lindhard, M. Scharff, and H. E. Schiott, K. Dan Vidensk. Selsk. Mat. Fys. Medd. 33, No. 14 (1963).

2. T. A. Mehlhorn, A Finite Material Temperature Model for Ion Energy Deposition in Ion-Driven ICF Targets, Sandia Laboratories, Albuquerque, New Mexico, Report No. SAND80-0038, May 1980.

3. D. Mosher, ERDA Summer Study of Heavy Ions for Inertial Fusion, LBL-5543, p. 39 (1976).

4. R. K. Nesbet and J. F. Ziegler, Appl. Phys. Lett. 31, 810 (1977).

5. J. W. Zink, Phys. Rev. 176, 279 (1968).

6. M. D. Brown and C. D. Moak, Phys. Rev. B 6, 90 (1972).

7. H. H. Andersen and J. F. Ziegler, Hydrogen-Stopping Powers and Ranges in All Elements, Pergamon Press (1977).

8. L. C. Northcliffe and R. F. Schilling, Nuclear Data Tables A7, 233 (1970).

9. D. J. Land and J. G. Brennan, Atomic Data and Nuclear Data Tables 22, 235 (1978).

10. K. A. Brueckner and N. Metzler, University of California, San Diego, LaJolla, Calif. 92093 (1980) (unpublished).

11. P. M. Campbell, Fast Ion Energy Loss in Dense Plasmas, (1980) (unpublished).

12. K. A. Brueckner and H. Brysk, Energy Loss of a Charged Particle in a Plasma, KMSF Document KMSF-U7 (1971).

13. D. Pines and D. Bohm, Phys. Rev. 85, 338 (1952).

14. J. D. Jackson, Classical Electrodynamics John Wiley and Sons, Inc., (1962), p. 643.

15. E. Nardi, E. Peleg, and Z. Zinamon, Phys. Fluids 21, 574 (1978).

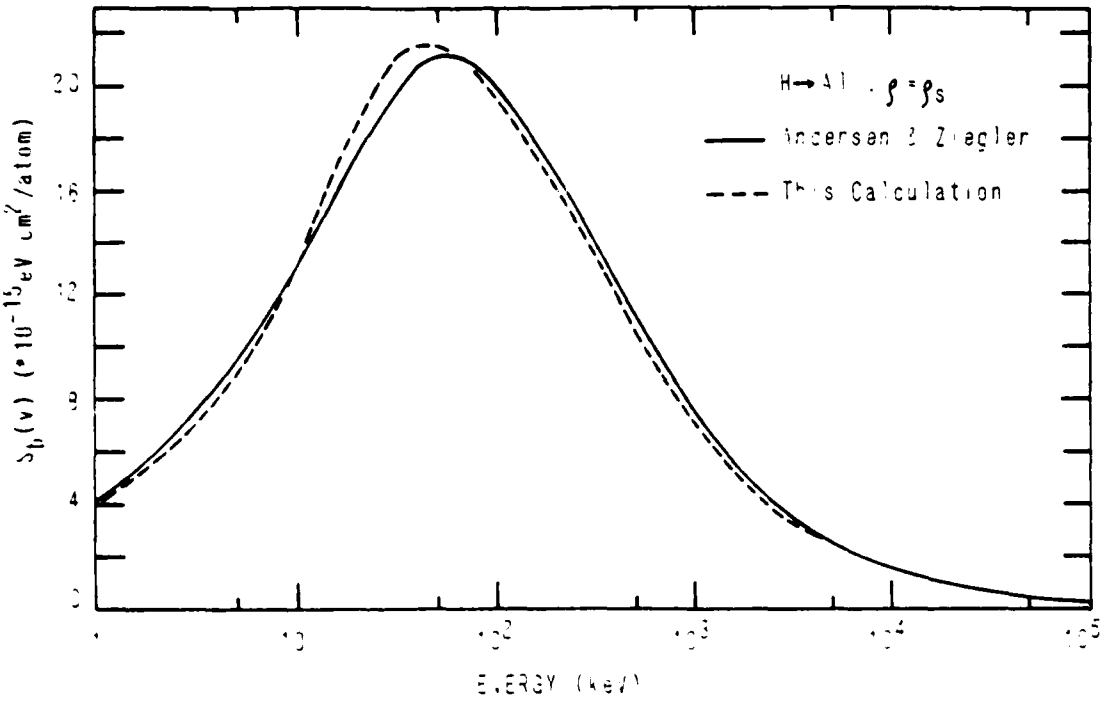

Fig. 1a — Cold target stopping cross section of solid density Al for H ions

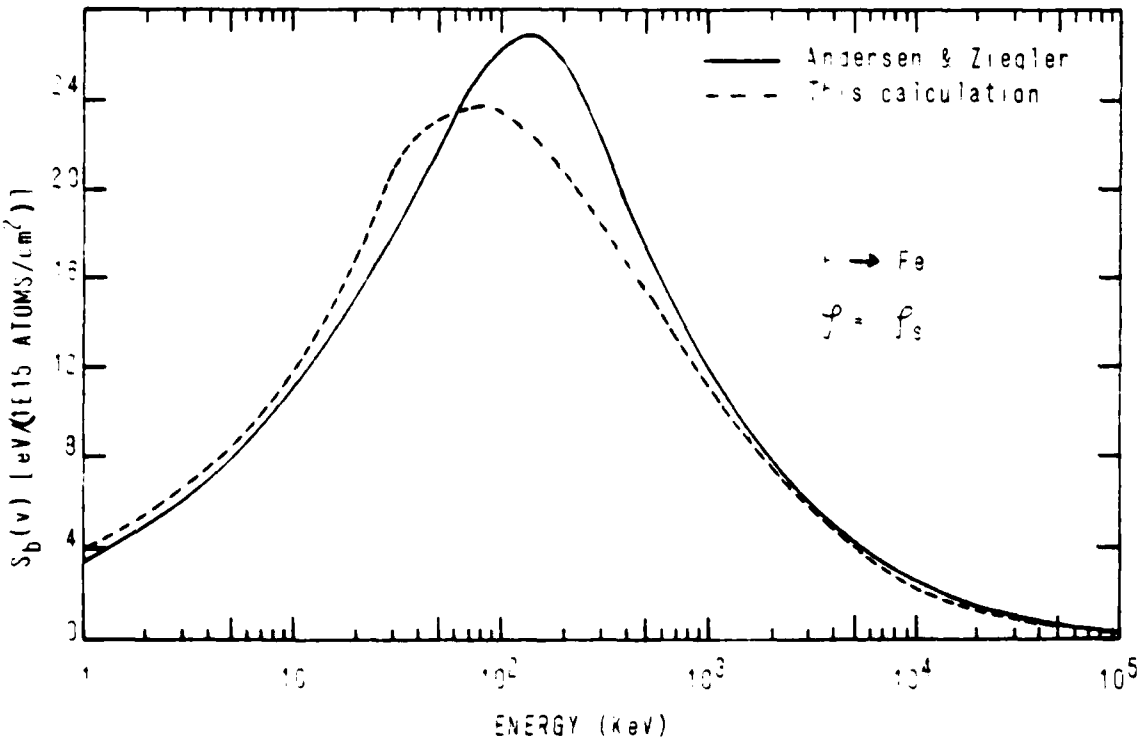

Fig. 1b — Cold target stopping cross section of solid density Fe for H ions

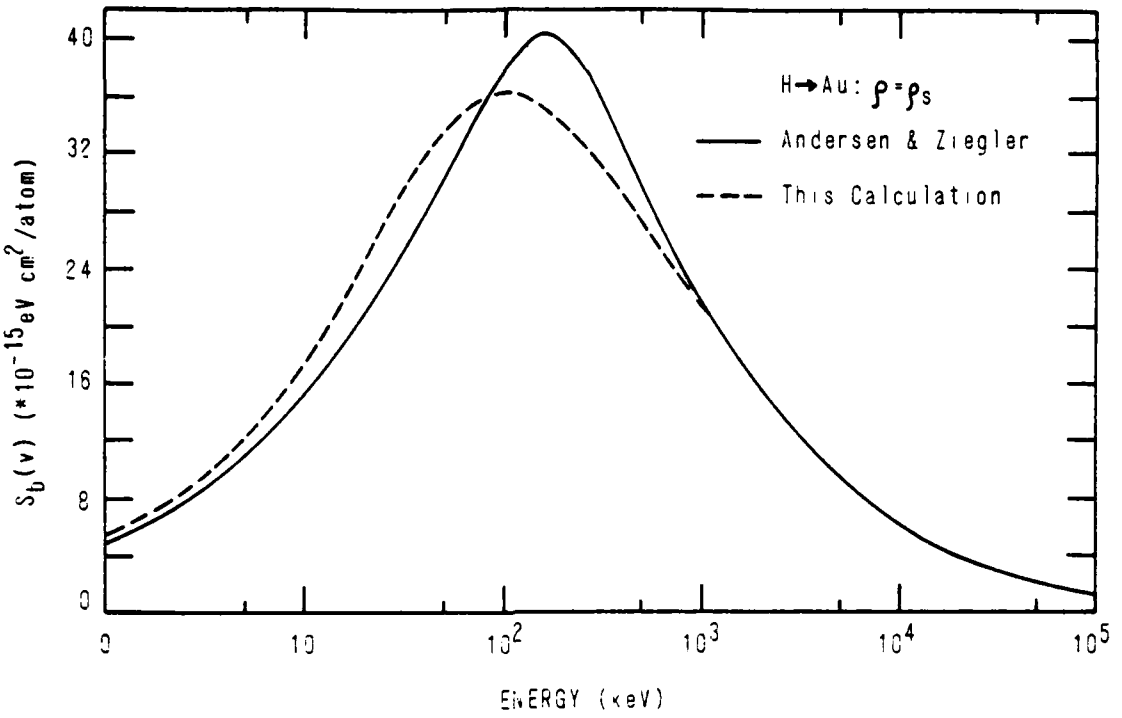

Fig. 1c — Cold target stopping cross section of solid density Au for H ions

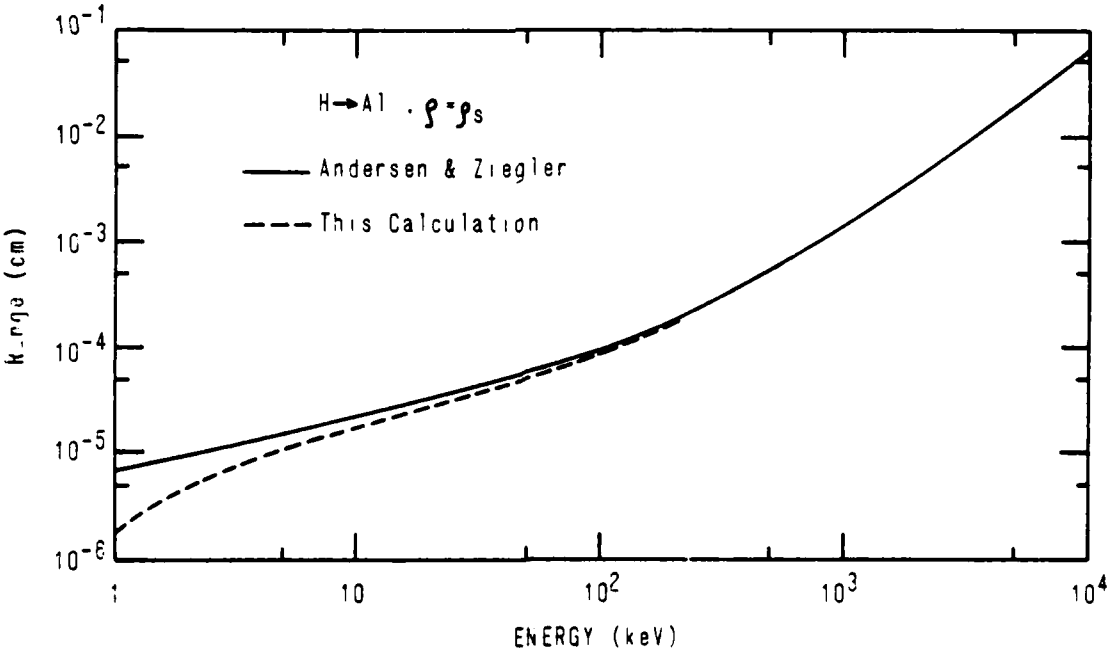

Fig. 1d — Range vs. energy of H ions in cold target, solid density Aℓ

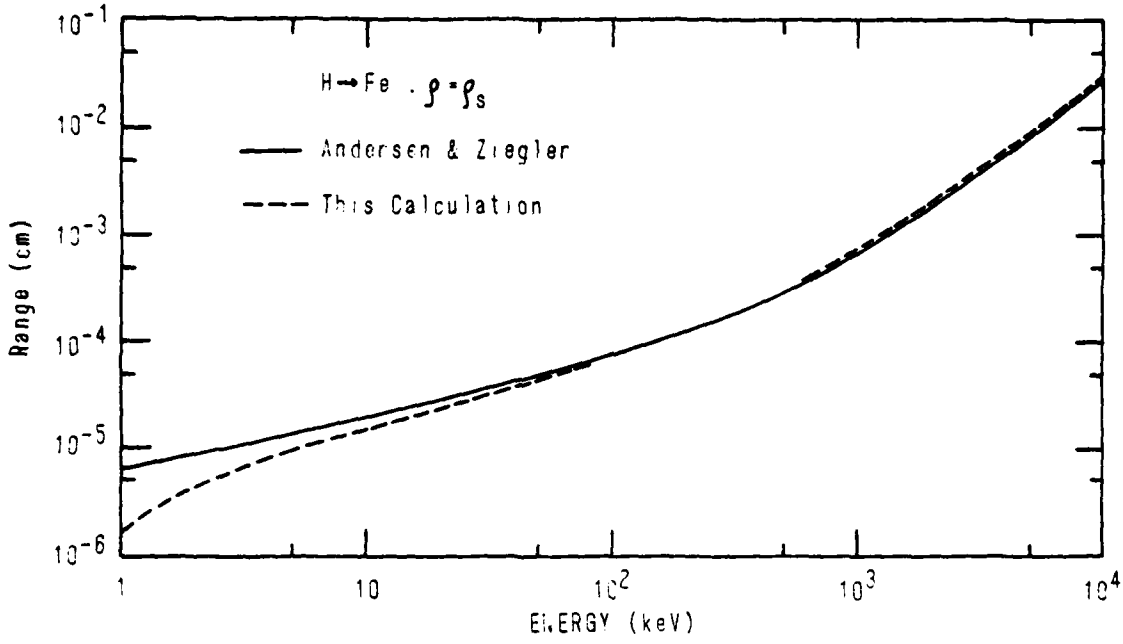

Fig. 1e — Range vs. energy of H ions in cold target, solid density Fe

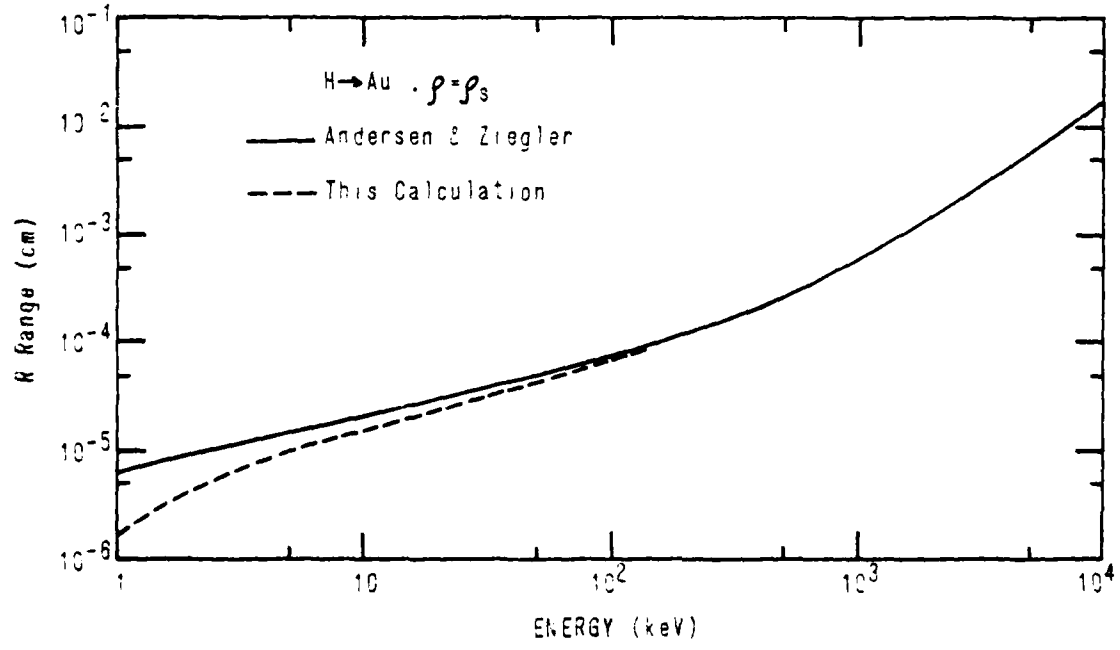

Fig. 1f — Range vs. energy of H ions in cold target, solid density Au

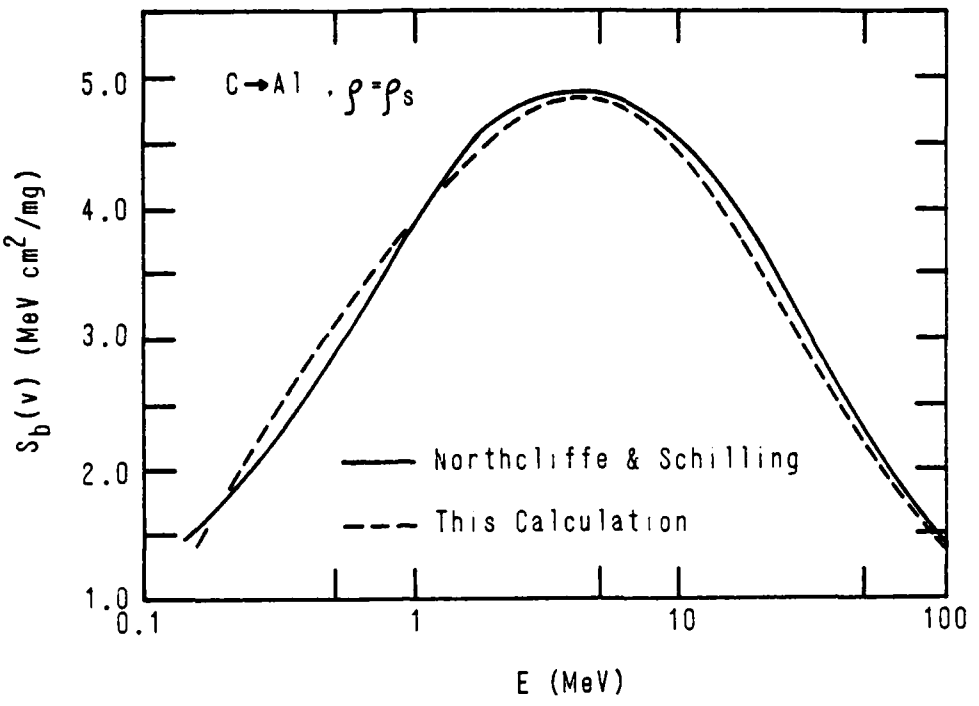

Fig. 2a — Cold target stopping cross section of solid density Aℓ for C ions

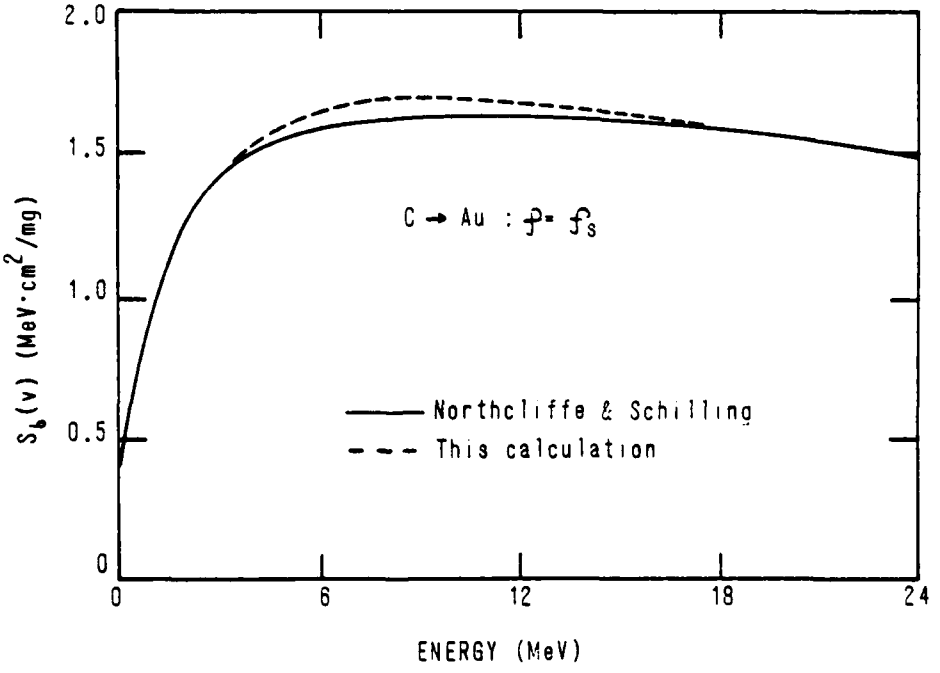

Fig. 2b — Cold target stopping cross section of solid density Au for C ions

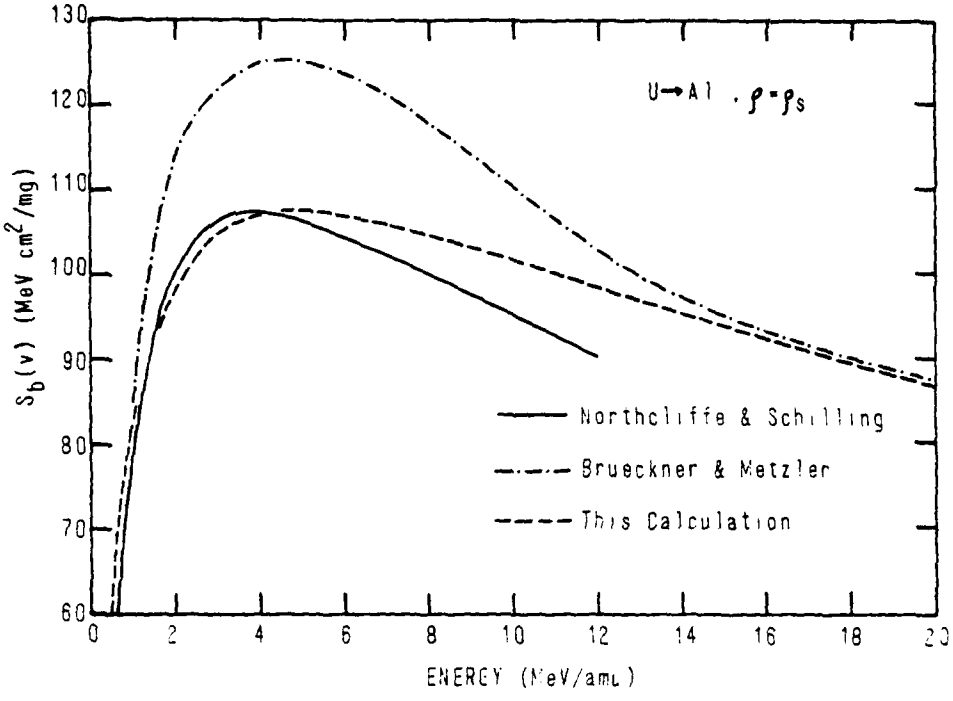

Fig. 3a — Cold target stopping cross section of solid density Al for U ions

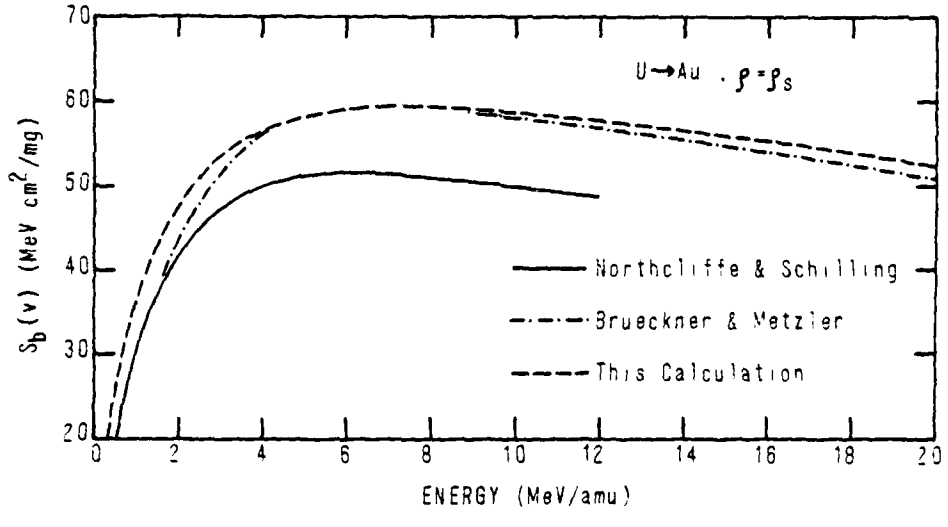

Fig. 3b — Cold target stopping cross section of solid density Au for U ions

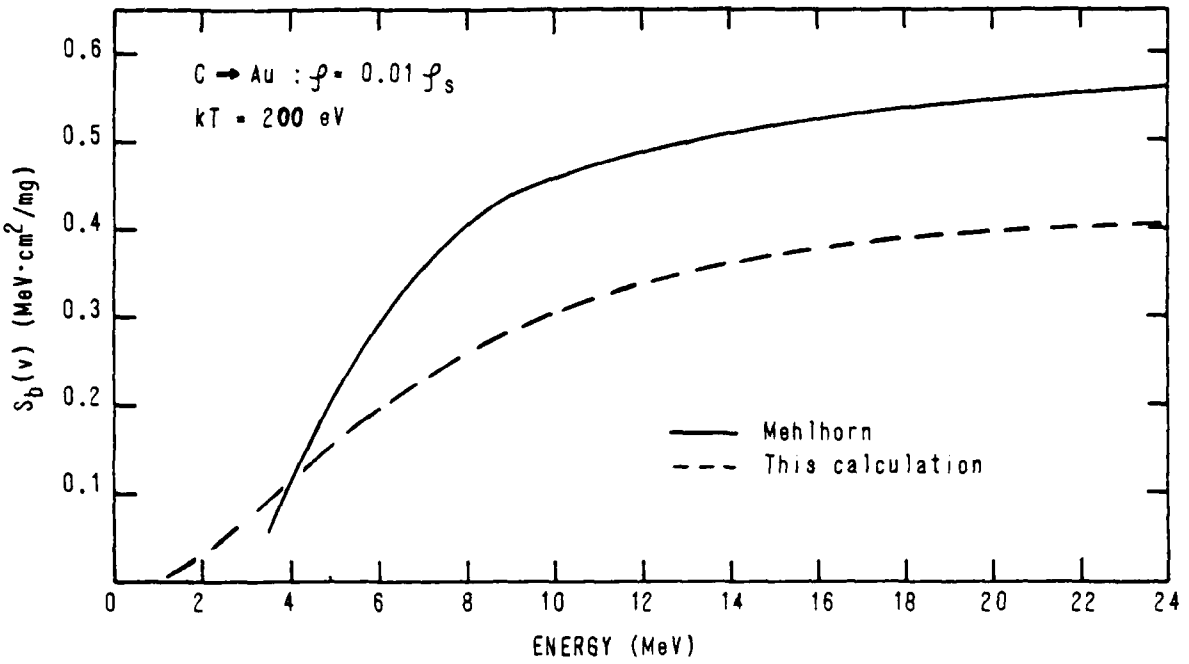

Fig. 4a — Bound electron stopping cross sections of Au at 0.01 times solid density and kT = 200 eV for C ions

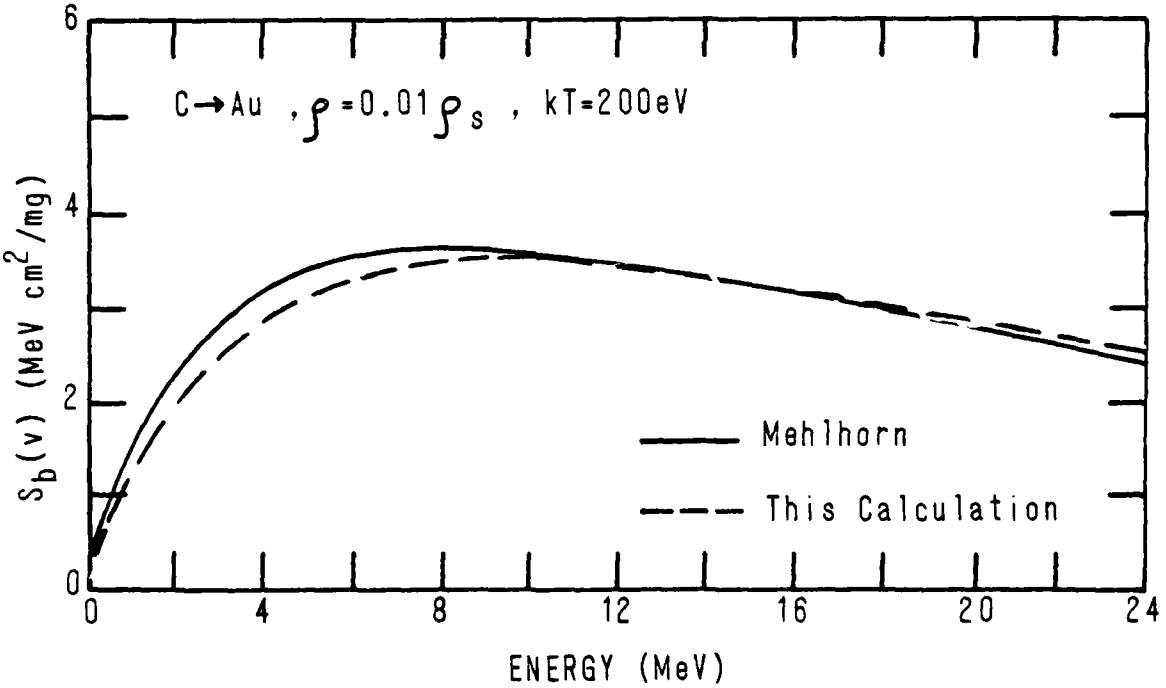

Fig. 4b — Free electron stopping cross section of Au at 0.01 times solid density and kT = 200 eV for C ions

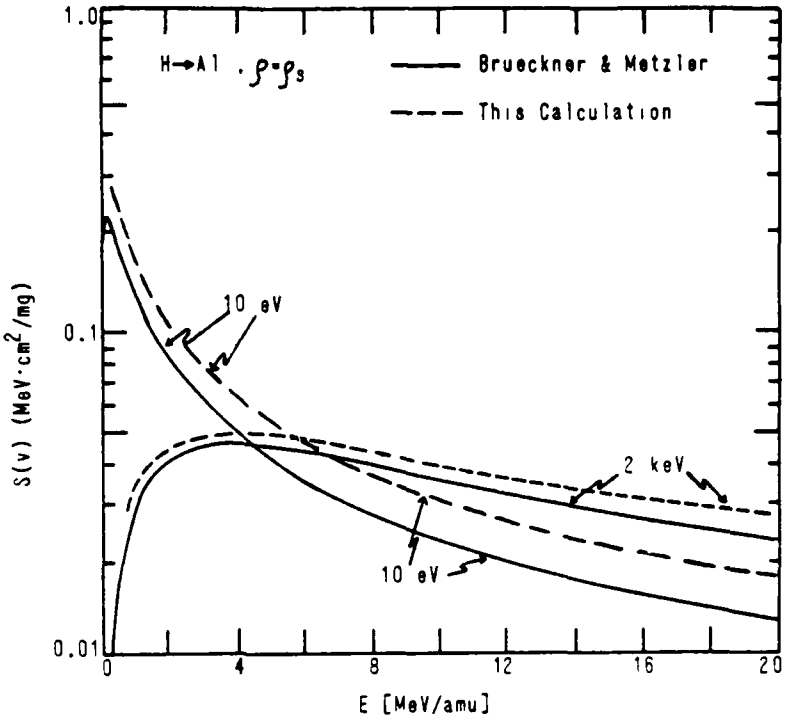

Fig. 5 — Total stopping cross section of solid density Aℓ at kT = 10 eV and kT = 2 keV for H ions

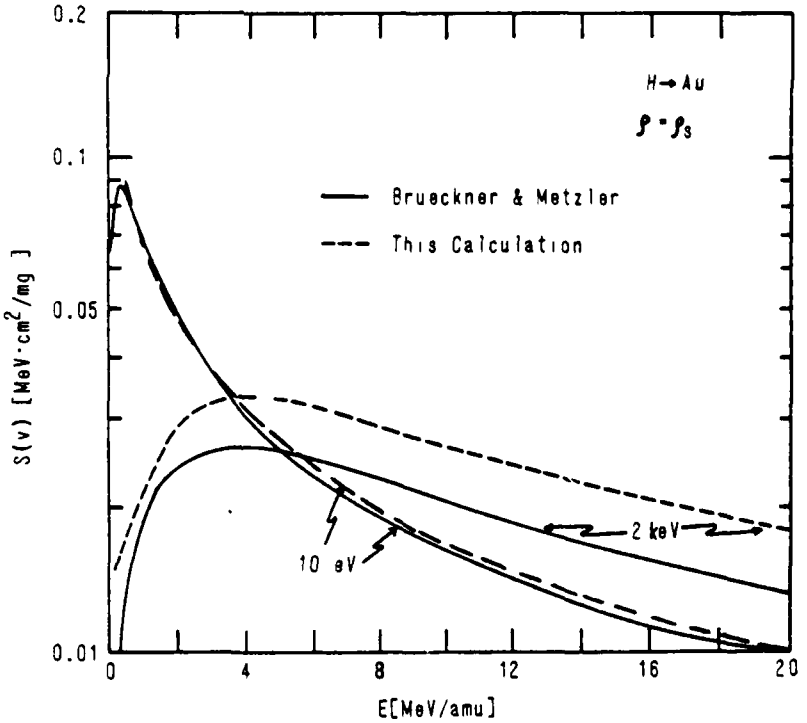

Fig. 6 — Total stopping cross section of solid density Au at kT = 10 eV and kT = 2 keV for H ions

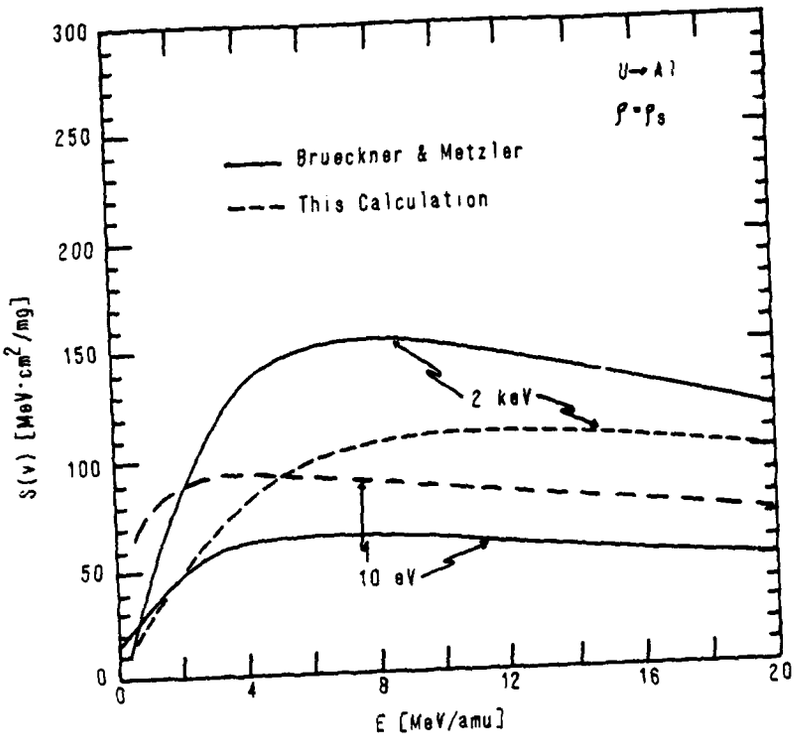

Fig. 7 — Total stopping cross section of solid density Aℓ at kT = 10 eV and kT = 2 keV for U ions

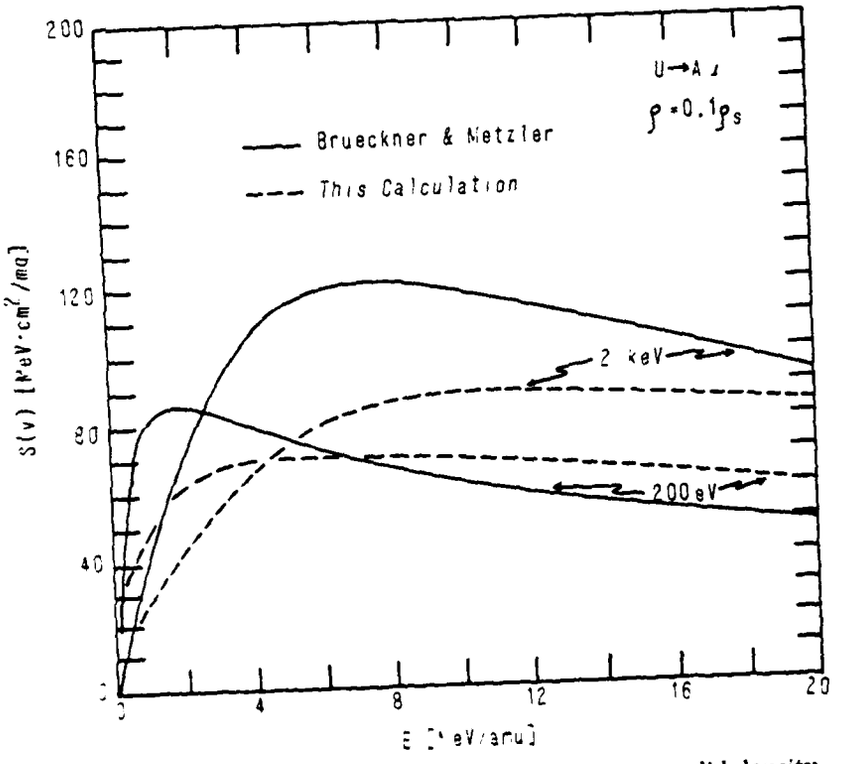

Fig. 8 — Total stopping cross section of Au at 0.1 times solid density and kT = 200 eV and kT = 2 keV for U ions

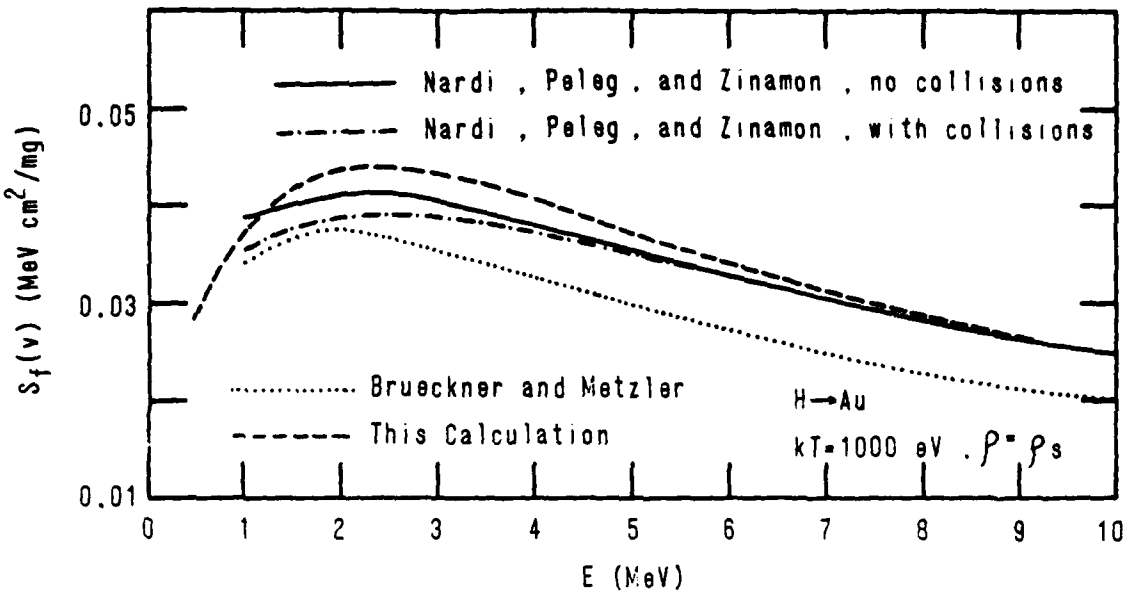

Fig. 9 — Free electron stopping cross sections for protrons in solid density Au at kT = 1 keV

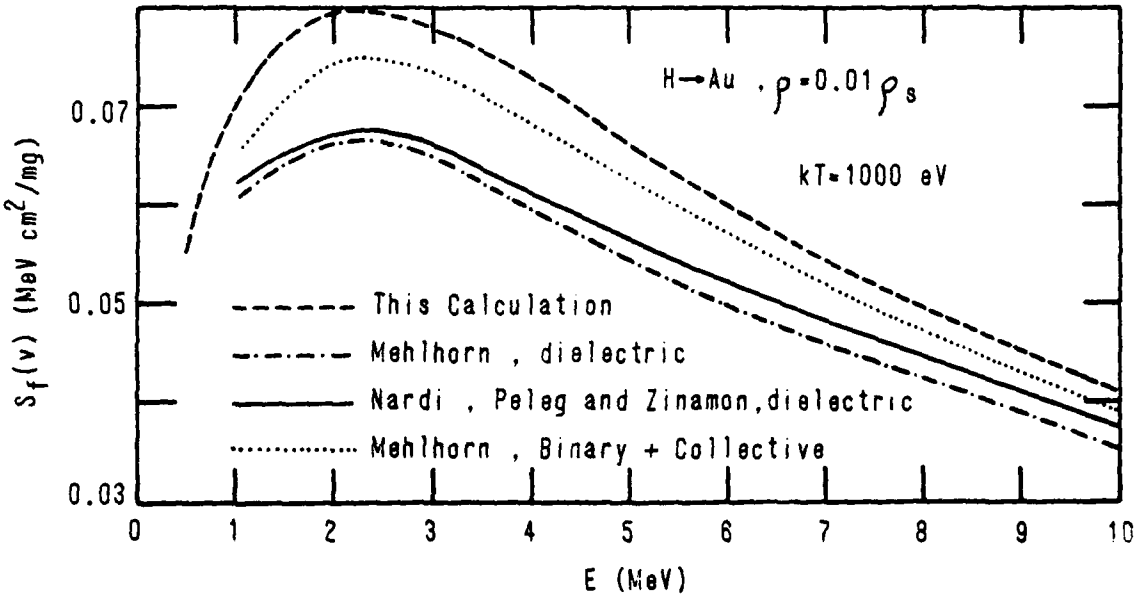

Fig. 10 — Free electron stopping cross sections for protrons in Au at 0.01 times solid density and kT = 1 keV

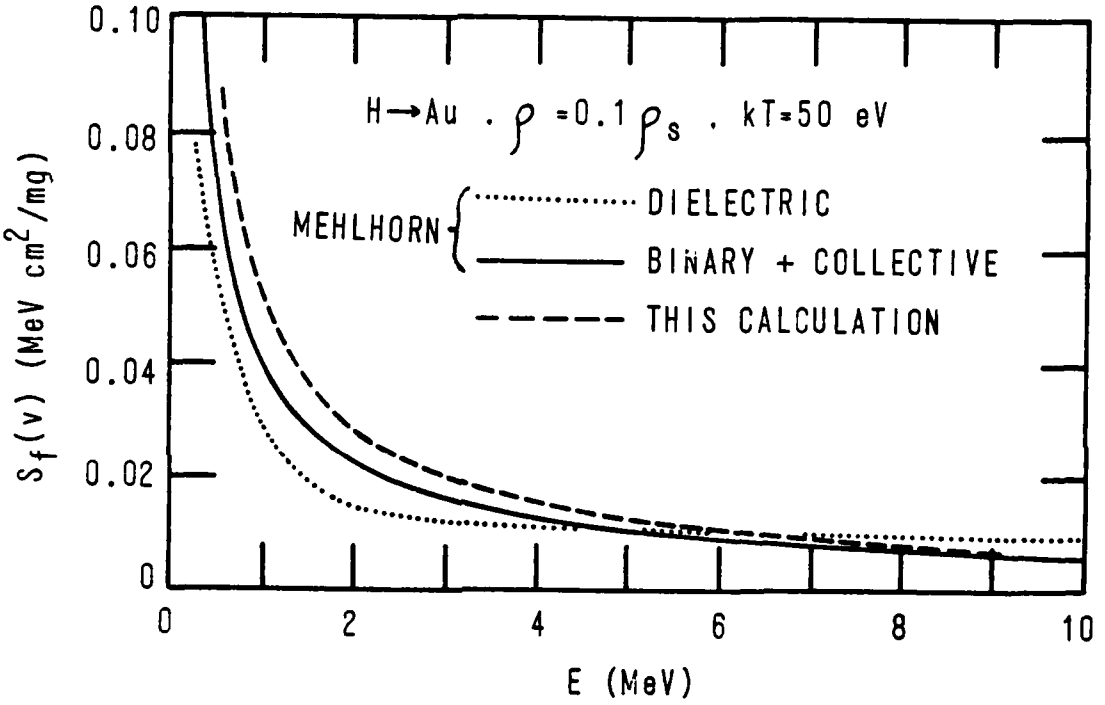

Fig. 11 — Free electron stopping cross sections for protrons in Au at 0.1 times solid density and kT = 50 eV

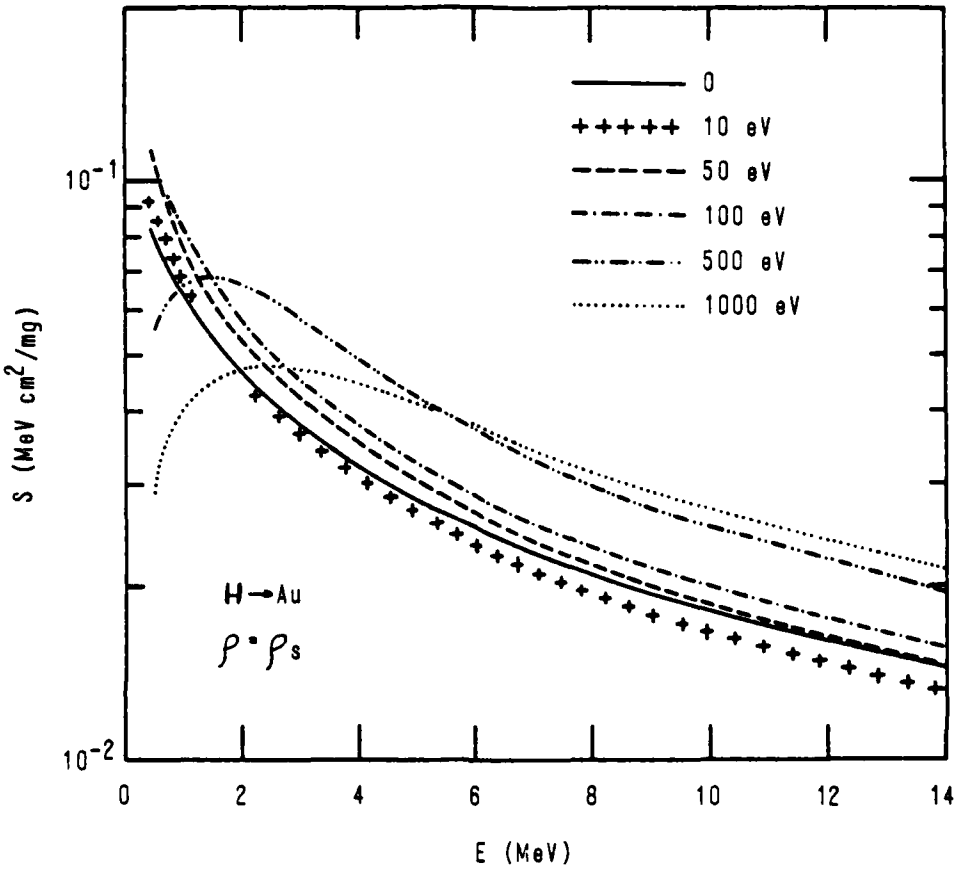

Fig. 12 — Total stopping cross sections for protrons in solid density Au at several values of kT

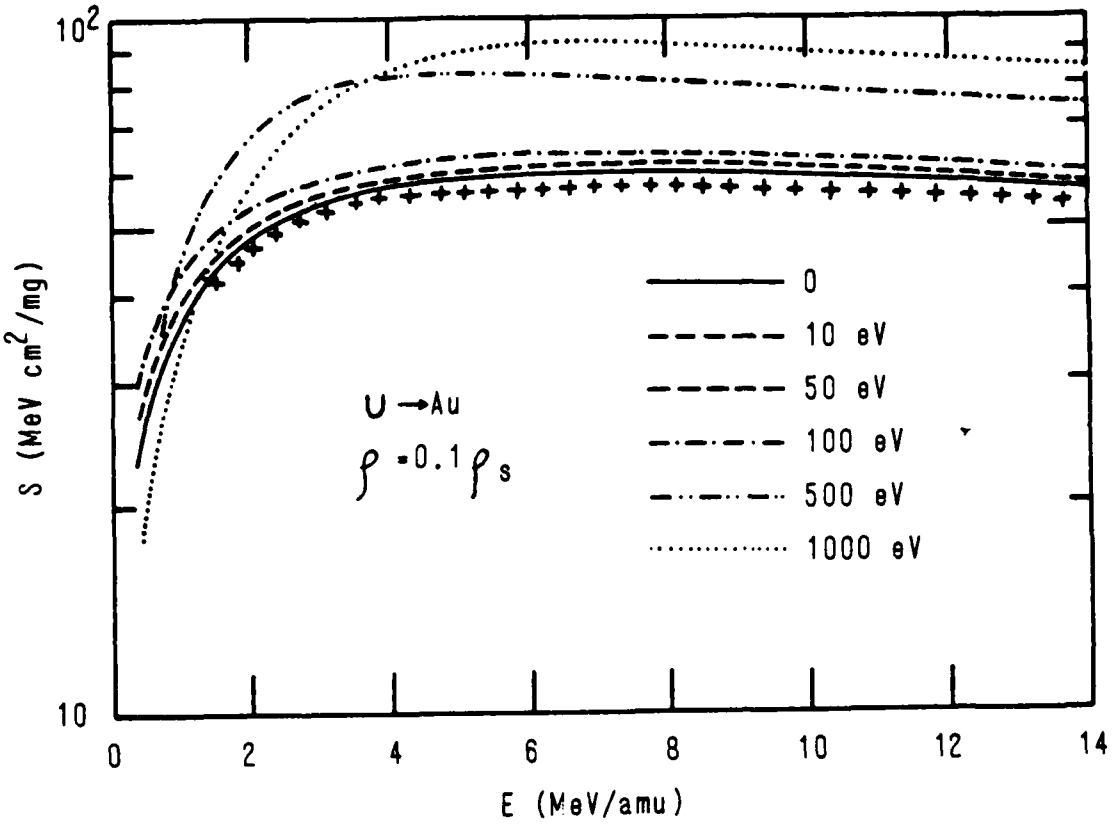

Fig. 13 — Total stopping cross sections for U ions in Au at 0.1 times solid density and at several values of kT

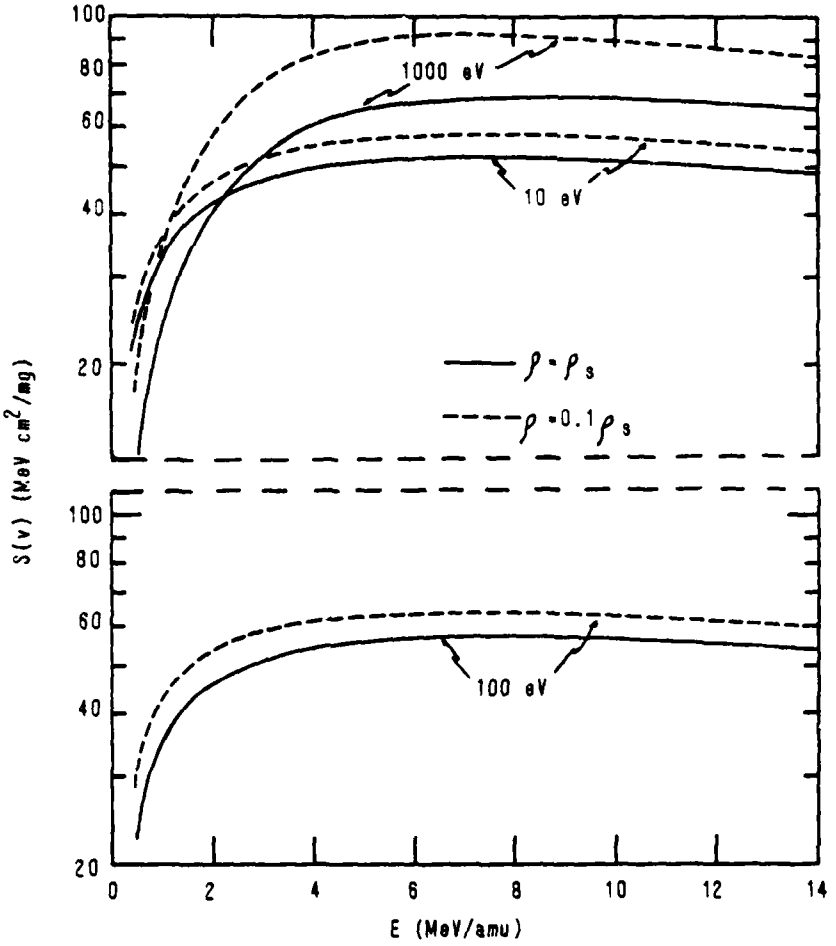

Fig. 14 — Comparison of total stopping cross sections for U ions in Au at solid density and 0.1 times solid density for dT = 10, 100, and 1000 eV

DISTRIBUTION LIST

Assistant to the Secretary of Defense
Atomic Energy
Washington, D.C. 20301

Attn: Executive Assistant

1 Copy
ATSDAE 600208
CNWDI

Defense Technical Information Center
Cameron Station
5010 Duke Street
Alexandria, Virginia 22314

(12 copies if open publication, otherwise 2 copies)
DDC 107200
CNWDI

Director
Defense Intelligence Agency
Washington, D.C. 20301
Attn: DT-1B R. Rubenstein

1 Copy
DIA 107300
CNWDI

Director
Defense Nuclear Agency
Washington, D.C. 20305
Attn: DDST (1 copy)
Attn: TITL (4 copies)
Attn: RAEV (1 copy)
Attn: STVI (1 copy)

DNA 107050
CNWDI

Commander
Field Command
Defense Nuclear Agency
Kirtland AFB, New Mexico 87115
Attn: FCPR

1 Copy
DNAFO 400361
CNWDI

Chief
Field Command
Livermore Division
Department of Defense
P. O. Box 808
Livermore, California 94550
Attn: FCPRL

1 Copy
LIVDNA 600158
CNWDI

Director
Joint Strat TGT Planning Staff
Offutt AFB
Omaha, Nebraska 68113
Attn: JSAS

1 Copy
JSTPS 600189
CNWDI

Under Secretary of Defense
For RSCH and ENGRG
Department of Defense
Washington, D.C. 20301
Attn: Strategic and Space Systems (OS)

1 Copy
USDRE 266200
CNWDI

Deputy Chief of Staff for RSCH DEV and ACQ
Department of the Army
Washington, D.C. 20301
Attn: DAMA-CSS-N

1 Copy
DCSRDA 265950
CNWDI

Commander
Harry Diamond Laboratories
Department of the Army
2800 Powder Mill Road
Adelphi, Maryland 20783
(CNWDI-Inner Envelope: Attn: DELHD-RBH)
Attn: P. Caldwell
Attn: DELHD-N-NP
Attn: DELHD-N-RBA J. Rosado
Attn: DELHD-N-TI (Tech. Lib)

HDL 1[illegible]
CNWDI

(1 copy each)

Commander
Redstone Scientific Information Center
U.S. Army R and D Command
Redstone Arsenal, Alabama 35809
Attn: Chief, Documents

REDSCI 600593
3 copies

Commander
U.S. Army Missile R and D Command
Redstone Arsenal, Alabama 35809
Attn: DRCPM-PE-EA

1 copy
AMICOM 040050
CNWDI

Commander
U.S. Army Nuclear and Chemical Agency
7500 Backlick Road
Building 2073
Springfield, Virginia 22150
Attn: Library

USANA 600492
CNWDI
1 Copy

Commander
U.S. Army Test and Evaluation Command
Aberdeen Proving Ground, Maryland 21005
Attn: DRSTE-EL

1 Copy
ATFCOM 041750
CNWDI

Commanding Officer
Naval Intelligence Support Center
4301 Suitland Road, Bldg. 5
Washington, D.C. 20390
Attn: NISC-45

1 COPY
NISC 252080

Commander
Naval Weapons Center
China Lake, California 93555
Attn: Code 233 (Tech. Lib.)

1 Copy
NWC 403019
CNWDI

Office of the Chief of Naval Operations
Washington, D.C. 20350
Attn: R. Blaise

1 Copy
CNO 264850
CNWDI

Officer in Charge
White Oak Laboratory
Naval Surface Weapons Center
Silver Spring, Maryland 20910
Attn: Code R-1 (1 copy)
Attn: Code F31 (1 copy)

NSWC 250650
CNWDI

Air Force Weapons Laboratory
Kirtland AFB, New Mexico 87117
Attn: SUL
Attn: CA
Attn: DYC
Attn: DT (1 copy each)
Attn: CA
Attn: DYP

AFWL 013150
CNWDI

Deputy Chief of Staff
Research, Development and Accounting
Department of the Air Force
Washington, D.C. 20330
Attn: AFRDQSM

1 Copy
USAFRD 611421

Space and Missile Systems Organization/DY
Air Force Systems Command
Post Office Box 92960
Worldway Postal Center
Los Angeles, California 90009
Attn: DYS (Technology)

1 Copy
SAMSO 611357
CNWDI

Space and Missile Systems Organization/IN
Air Force Systems Command
Post Office Box 92960
Worldway Postal Center
Los Angeles, California 90009
Attn: IND D. Muskin (Intelligence)

1 Copy
SAMSO 611392
CNWDI

Space and Missile Systems Organization/MN
Air Force Systems Command
Norton AFB, California 92409
Attn: MNNH (Minuteman)

1 Copy
NORTON 600190
CNWDI

Space and Missile Systems Organization/SK
Air Force Systems Command
Post Office Box 92960
Worldway Postal Center
Los Angeles, California 90009
Attn; SKF P. Stadler (Space Comm. Systems)

1 Copy
SAMSO 611387
CNWDI

AVCO Research and Systems Group
201 Lowell Street
Wilmington, Massachusetts 01887
Attn: Library A830

1 Copy
AVNIL 403936
Fac Clear T CNDWI
Stor Capability T

BDM Corporation
7915 Jones Branch Drive
McLean, Virginia 22101
Attn: Corporate Library)

1 Copy
BDMVA 404435
Fac Clear T CNWDI
Stor Capability T

Boeing Company
P. O. Box 3707
Seattle, Washington 98124
Attn: Aerospace Library

1 Copy
BOE 059600
Fac Clear T CNWDI
Stor Capability T

Dikewood Industries, Inc.
1009 Bradbury Drive, S.E.
Albuquerque, New Mexico 87106
Attn: L. Davis

1 Copy
DIKEWD 112850
Fac Clear T CNWDI
Stor Capability T

EG and G Washington Analytical Services Center, Inc.
P. O. Box 10218
Albuquerque, New Mexico 87114
Attn: Library

1 Copy
EGGALB 388316
Fac Clear T CNWDI
Stor Capability S

General Electric Company
Space Division
Valley Forge Space Center
P. O. Box 8555
Philadelphia, Pa. 19101
Attn: J. Peden

1 Copy
GESD 149070
Fac Clear T CNWDI
Stor Capability T

General Electric Company - Tempo
Center for Advanced Studies
816 State Street
P. O. Drawer QQ
Santa Barbara, California 93102
Attn: DASIAC

1 Copy
TEMPO 346420
Fac Clear T CNWDI
Stor Capability T

Institute for Defense Analyses
400 Army-Navy Drive
Arlington, Va. 22202
Attn: Classified Library

1 Copy
IDA 179350
Fac Clear T CNWDI
Stor Capability T

IRT Corporation
P.O. Box 81087
San Diego, California 92138
Attn: R. Mertz

1 Copy
IRT 601410
Fac Clear T CNWDI
Stor Capability T

JAYCOR
1401 Camino Del Mar
Del Mar, California 92014
Attn: E. Wenaas

1 Copy
JAYCA 611545
Fac Clear T CNWDI
Stor Capability S

JAYCOR
205 S Whiting Street, Suite 500
Alexandria, Virginia 22304
Attn: R. Sullivan

1 Copy
JAYVA 611580
Fac Clear T CNWDI
Stor Capability S

KAMAN Sciences Corp.
P. O. Box 7463
Colorado Springs, Colorado 80933
Attn: J. Hoffman
Attn: A. Bridges
Attn: D. Bryce
Attn: W. Ware
(1 copy each)

KN 195000
FAC Clear T CNWDI
Stor Capability T

Lawrence Livermore National Laboratory
University of California
P. O. Box 808
Livermore, California 94550
Attn: DOC CDN for L-545 J. Nickolls
Attn: DOC CDN for L-153
Attn: DOC CDN for L-47 L. Wouters
Attn: DOC CDN for Technical Infor. Dept. Lib.

LLI 204150
CNWDI

(1 copy each)

Lockheed Missiles and Space Co., Inc.
P. O. Box 504
Sunnyvale, California 94086
Attn: S. Taimlty

LMSC 210120
Fac Clear T CNWDI
Stor Capability T

Lockheed Missiles and Space Co., Inc.
3251 Hanover Street
Palo Alto, California 94304
Attn: L. Chase

1 Copy
LMSCPA 210110
Fac Clear T CNWDI
Stor Capability T

Maxwell Laboratory, Inc.
9244 Balboa Avenue
San Diego, California 92123
Attn: A. Kolb
Attn: W. Clark
Attn: J. Pearlman

1 Copy each
MAXLAB 387218
Fac Clear T CNWDI
Stor Capability S

McDonnell Douglas Corp.
5301 Bolsa Avenue
Huntington Beach, California 92647
Attn: S. Schneider

1 Copy
MDCHB 404770
Fac Clear T CNWDI
Stor Capability T

Mission Research Corp.
P.O. Drawer 719
Santa Barbara, California 93102
Attn: C. Longmire
Attn: W. Hart

1 Copy each
MRC 600289
Fac Clear T CNWDI
Stor Capability S

Mission Research Corp.-San Diego
P. O. Box 1209
La Jolla, California 92038
Attn: Victor J. Van Lint

1 Copy
MRCVLN 400205
Fac Clear T CNWDI
Stor Capability S

Northrop Corporation
Northrop Research and Technology Center
1 Research Park
Palos Verdes Peninsula, California 90274
Attn: Library

1 Copy
NCPVP
Fac Clear T CNWDI
Stor Capability S

Northrop Corporation
Electronic Division
2301 120th Street
Hawthorne, California 90250
Attn: V. Damarting

1 Copy
NOREL 600302
Fac Clear T CNWDI
Stor Capability T

Physics International Company
2700 Merced Street
San Leandro, California 94577

Attn: C. Stallings
Attn: B. Bernstein
E. Goldman

1 Copy each
PIC 282760
Fac Clear S CNWDI
Stor Capability S

R and D Associates
P. O. Box 9695
Marina Del Rey, California 90291
Attn: W. Graham, Jr.
Attn: C. MacDonald

1 Copy each
RDA 600466
Fac Clear T CNWDI
Stor Capability T

Sandia National Laboratories
P.O. Box 5800
Albuquerque, New Mexico 87115
Attn: Doc Con For G. Yonas
Attn: Doc Con For 3141

1 Copy each
SANALB 315800
CNWDI

Science Applications, Inc.
P. O. Box 2351
La Jolla, California 92038
Attn: J. Beyster

SAI 603100
Fac Clear T CNWDI
Stor Capability T

Spire Corporation
P. O. Box D
Bedford, Massachusetts 01730
Attn: R. Little

SPI 600215
Fac Clear T CNWDI
Stor Capability S

SRI International
333 Ravenswood Avenue
Menlo Park, California 94025
Attn: S. Dairiki

SRI 332500
Fac Clear T CNWDI
Stor Capability T

Systems, Science and Software, Inc.
P. O. Box 1620
La Jolla, California 92038
Attn: A. Wilson

Se 399507
Fac Clear T CNWDI
Stor Capability S

Texas Tech University
P. O. Box 5404, North College Station
Lubbock, Texas 79417
Attn: T. Simpson

TXTECU 405703
Fac Clear S
Stor Capability S

TRW Defense and Space Systems Group
One Space Park
Redondo Beach, California 90278
Attn: Technical Information Center

1 Copy
TRWRB 354595
Fac Clear T CNWDI
Stor Capability T

Vought Corporation
Michigan Division
38111 Van Dyke Road
Sterling Heights, Maine 48077
Attn: Technical Information Center
(Formerly LTV Aerospace Corp.)

1 Copy
Vought 611546
Fac Clear T
Stor Capability T

Naval Research Laboratory
Washington, D.C. 20375

Code 4700 25 copies

Code 4707 50 copies


DAT
FILM